



Short communication

Nitridated Si–Ti–Ni alloy as an anode for Li rechargeable batteries



Taeseup Song^{a,1}, Ki Chun Kil^{b,1}, Yeryoung Jeon^b, Sangkyu Lee^a, Woo Cheol Shin^c,
Byungjoo Chung^c, Kyungjung Kwon^{d,2}, Ungyu Paik^{b,*}

^a Department of Materials Science & Engineering, Hanyang University, Seoul 133-791, Republic of Korea

^b WCU Department of Energy Engineering, Hanyang University, Seoul 133-791, Republic of Korea

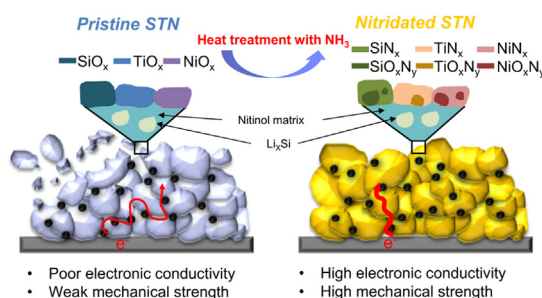
^c Energy 2Lab, Corporate R&D Center, Samsung SDI Co. Ltd., 428-5, Gonsse-dong, Giheung-gu, Yongin-si, Gyeonggi-do 446-577, Republic of Korea

^d Department of Energy & Mineral Resources Engineering, Sejong University, Seoul 143-747, Republic of Korea

HIGHLIGHTS

- Nitridated Si–Ti–Ni alloy was obtained by the NH_3 nitridation of Si–Ti–Ni alloy.
- Nitridated Si–Ti–Ni electrode showed high reversible capacity and rate capability.
- Improvements are attributed to nitride compounds which benefits both mechanics and kinetics.

GRAPHICAL ABSTRACT



ARTICLE INFO

Article history:

Received 3 October 2013

Received in revised form

7 December 2013

Accepted 9 December 2013

Available online 17 December 2013

Keywords:

Silicon alloy

Nitridation

Anode

Li ion batteries

ABSTRACT

Nitridated Si–Ti–Ni (STN) ternary alloy as an anode for lithium ion batteries is prepared by the NH_3 nitridation of STN alloy. The nitridated STN electrode shows 14% increased reversible capacity and 4 times higher rate capability at 3 C compared to those of pristine STN electrode. These improvements are attributed to the formation of nitride compounds (such as $\text{SiN}_x/\text{SiN}_x\text{O}_y$, $\text{TiN}_x/\text{TiN}_x\text{O}_y$ and $\text{NiN}_x/\text{NiN}_x\text{O}_y$) on STN alloy, which benefits both mechanics and kinetics.

© 2013 Elsevier B.V. All rights reserved.

1. Introduction

Silicon is a promising candidate as an anode material for lithium-ion batteries (LIBs) due to its high theoretical capacity of

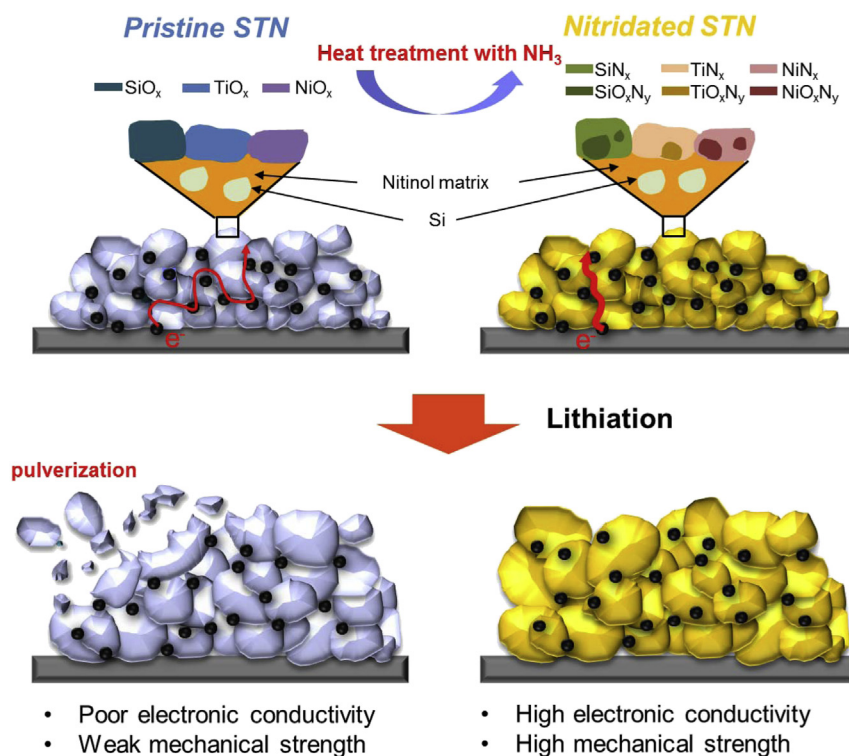
4200 mAh g^{-1} and relatively low working potential [1,2]. However, poor cycle performance, which results from the pulverization of Si active material and the breakdown of electrical conduction pathways caused by a large volumetric change during cycling, limits its practical use [3]. Considerable effort has been devoted to improve the cycle performance by engineering the electrode configuration including the dimension, geometry and composition. Nanostructured Si materials, such as nanoparticles [4], nanowires [5], and Si nanoparticle-decorated Si nanowire [6], showed improved capacity retention compared to that of a bulk Si due to a smaller absolute volume change and mechanical stress induced during

* Corresponding author. Tel.: +82 2 2220 0502; fax: +82 2 2281 0502.

E-mail addresses: kfromberk@gmail.com (K. Kwon), upaik@hanyang.ac.kr (U. Paik).

¹ Both authors contributed equally to this work.

² Tel.: +82 2 3408 3947; fax: +82 2 3408 4344.



Scheme 1. Schematic illustration of pristine STN and nitridated STN electrodes.

cycling [2–7]. Porous nanostructured materials, such as porous three-dimensional nanorod array [8], Si nanotube array [9] and hierarchical micro/nano porous silicon [10], have been also extensively explored. Their porous morphology and high ratio of surface area to volume enable a facile strain relaxation, which leads to significant improvement in electrochemical performances, especially cycle performance. Although these Si nanostructures with unique geometries showed promise, the expensive cost and difficulty in the synthesis of these nanostructured materials limit their practical use in commercial products. Alternative approach is the incorporation of nano-sized Si particles into a shape memory alloy composed of inactive phase metals to lithium. The Si–Ti–Ni (STN) ternary alloy is a representative form of such kinds of materials. Nitinol matrix, nickel–titanium (Ni–Ti) alloy, is an inactive phase to lithium, and it has high elastic characteristics which could accommodate effectively the large volume change of embedded Si without mechanical degradation, enabling a robust cycle performance [11,12]. Furthermore, the synthesis method is simple and cost-effective for large scale production. Jung et al. reported that ultra-fine sized Si embedded into the Ni–Ti matrix phase electrode shows reversible capacity of 907 mAh g^{-1} and cycle performance of 77% for 50 cycles [11]. Son et al. prepared nano-Si particles embedded into a matrix of $\text{Ti}_4\text{Ni}_4\text{Si}_7$ using melt spinning method. Nano-Si particles embedded into a matrix of $\text{Ti}_4\text{Ni}_4\text{Si}_7$ electrode delivers initial discharge capacity of 1325 mAh g^{-1} , charge capacity of 1158 mAh g^{-1} , and cycle performance of 78% for 50 cycles [12]. However, there exist several challenges for the practical use of STN as an anode material. For instance, various native oxides, such as SiO_x , TiO_x and NiO_x , are necessarily formed on the surface of STN particles, which induces large irreversible capacity and poor rate capability caused by low electrical conductivity [11,12]. These issues should be addressed to successfully replace current carbon-based anode with the STN-based anode and realize LIBs with high energy density and power density.

Here we report nitridated STN ternary alloy as an anode material for high energy and power density LIBs with robust performances. Nitridated STN was simply prepared by the heat treatment of STN powder under NH_3 flow. Various nitride compounds ($\text{SiN}_x/\text{SiO}_x\text{N}_y$, $\text{TiN}_x/\text{TiO}_x\text{N}_y$ and $\text{NiN}_x/\text{NiO}_x\text{N}_y$) converted from the native metal oxides could be formed on the surface of STN powder after the nitridation process (Scheme 1). These nitride compounds would be beneficial to the electrochemical performances of STN-based electrodes. The $\text{SiN}_x/\text{SiO}_x\text{N}_y$ and $\text{TiN}_x/\text{TiO}_x\text{N}_y$ compounds have much higher mechanical strength and electronic conductivity compared to their metal oxide forms, which enables significant improvements in both mechanics and kinetics [13]. Furthermore, the $\text{NiN}_x/\text{NiO}_x\text{N}_y$ compound shows higher specific capacity and better reversibility in electrochemical behavior than NiO_x form [14]. The physicochemical properties for the oxide, nitride and oxynitride in literature are summarized in Table S1. In this study, we demonstrate that significant improvements of the STN anode material in electrochemical performances could be achieved by its surface modification with nitride compounds via simple nitridation process.

2. Experiment

STN powder (MK electron) with an atomic ratio of 66%(Si)–17%(Ti)–17%(Ni) was used as a starting material. For the synthesis of nitridated STN, pristine STN was loaded into a tube furnace. And then, the furnace was heated up to 500°C and maintained for 2 h under the flow of NH_3 gas (200 sccm). After that, the sample was cooled down to room temperature. To prepare electrodes, pristine or nitridated STN and graphite as active materials, Ketjen black as a conducting agent and modified carboxymethyl cellulose (CMC) as a binder were used in a weight ratio of 88:4:8. The mixing process was conducted by Thinky mixer at 2000 rpm for 10 min. The prepared slurry was coated onto a copper current collector by doctor blade to make electrodes. To evaluate the electrochemical

performance, 2032R type coin cells were fabricated, comprising pristine STN or nitridated STN mentioned above as working electrodes, a pure lithium metal foil as a counter electrode, 1.5 M LiPF_6 in ethylene carbonate/diethylene carbonate/fluoroethylene carbonate (EC/DEC/FEC, 5:70:25 vol %) as an electrolyte and a polypropylene (PP) separator. The coin-type half cells were cycled in the voltage range between 0.01 and 2 V using a battery cycle tester (TOSCAT 3000, Toyo Systems, Tokyo, Japan). The cycle performance and rate capability of the cells were evaluated in a constant current–constant voltage (CC–CV) mode and constant current (CC) mode, respectively. Pristine STN and nitridated STN powder were characterized using a field emission scanning electron microscope (FE-SEM, JEOL JSM-7600F), a field emission transmission electron microscope (FE-TEM, JEOL JEM-2100F), scanning TEM (STEM, JEOL JEM-2100F), X-ray photoelectron spectrometer (XPS, VG microtech ESCA2000) and X-ray diffraction (XRD, Rigaku D/MAX RINT-2000).

3. Results and discussion

Fig. 1 shows the electron microscopy images for the pristine STN and the nitridated STN powders. As shown in the field emission scanning electron microscope (FE-SEM) image (Fig. 1(a)), the pristine STN powder has a wide range of particle size distribution from 1 μm to 10 μm . The detailed morphology of pristine STN powder was further characterized using a transmission electron microscope (TEM). The Low magnification TEM image (Fig. 1(b)) shows a clear variation in the brightness between Si–Ti–Ni alloy matrix and Si domain due to the different scattering ability of each metal. It is observed that Si domains with the diameter of 20 nm (relatively bright dots) are uniformly embedded in the Ni–Ti matrix. The morphology of homogeneously distributed Si domains in the matrix with high elastic characteristics is beneficial to the cycle performance *via* facile strain relaxation and improved mechanical properties. HR-TEM images of bare STN and nitridated STN particles clearly show amorphous layers on their surface regardless of the nitridation treatment (Fig. S3). Fig. 1(c) shows the scanning transmission electron microscope (STEM) image and the compositional line profile for the STN particle. The signals corresponding to four elements (Si, Ti, Ni and O) are uniformly observed along the yellow

line (in the web version) in Fig. 1(c). The signal corresponding to Si shows the highest intensity compared to the other elements. The intensities for Ni and Ti element signals are identical. Very weak O element signal is detected due to the native oxide layer formed on the surface of STN particle. Fig. 1(d) and (e) shows the SEM and the low magnification TEM images for the nitridated STN particles, respectively. A noticeable difference in size and morphology was not observed in the nitridated STN. However, compositional line profile for the nitridated STN particle (Fig. 1(f)) reveals that nitrogen signal is newly generated while maintaining the signals of the other elements. The intensity of nitrogen signal is similar to that of oxygen signal.

X-ray diffractometer (XRD) and X-ray photoelectron spectroscopy (XPS) were employed to investigate a change in crystal phase and surface composition of STN powder before and after the nitridation process, respectively. XRD result clearly shows a structural change of STN powder after the nitridation process (Fig. S1). In the case of pristine STN powder, all diffraction patterns are assigned to crystalline Si and Ti–Ni alloy. After nitridation, the diffraction patterns related to Si and Ni–Ti alloy become sharp with high intensity. The heat treatment during the nitridation process results in the stimulation of crystallographic ordering of STN powder, which induces new diffraction peaks generated at 22.4° , 34.6° , 58.6° , 60.6° , 62.5° , 64.5° and 71.2° . Although we could not find the crystalline materials that match newly generated peaks in JCPDS database, they might represent nitridated Si–Ti or Si–Ni binary/ternary intermetallic compounds. Fig. S2 shows the XPS spectra for both pristine STN and nitridated STN powders. It is clear that the N 1s peaks were developed after the nitridation process. The N 1s peaks correspond to the typical binding energy of nitride compounds. In the XPS spectra of Ti 2p, a noticeable peak shift in the range of 456–457 eV was observed after nitridation, which is closely related to TiN_x and TiO_xN_y [15]. In the XPS result for Si 2p of the pristine STN powder, the peaks located at ~ 102.5 eV and ~ 99 eV are assigned to Si–O and Si–Si bonding, respectively [16]. After the nitridation process, the peak located at ~ 102.5 eV was broadened and shifted to the 100.5–101 eV range, corresponding to Si–N bonding [17]. Although a slight peak shift is observed in the XPS spectrum of Ni 2p after the nitridation process, this shift may not support the formation of $\text{NiN}_x/\text{Ni}_x\text{O}_y$.

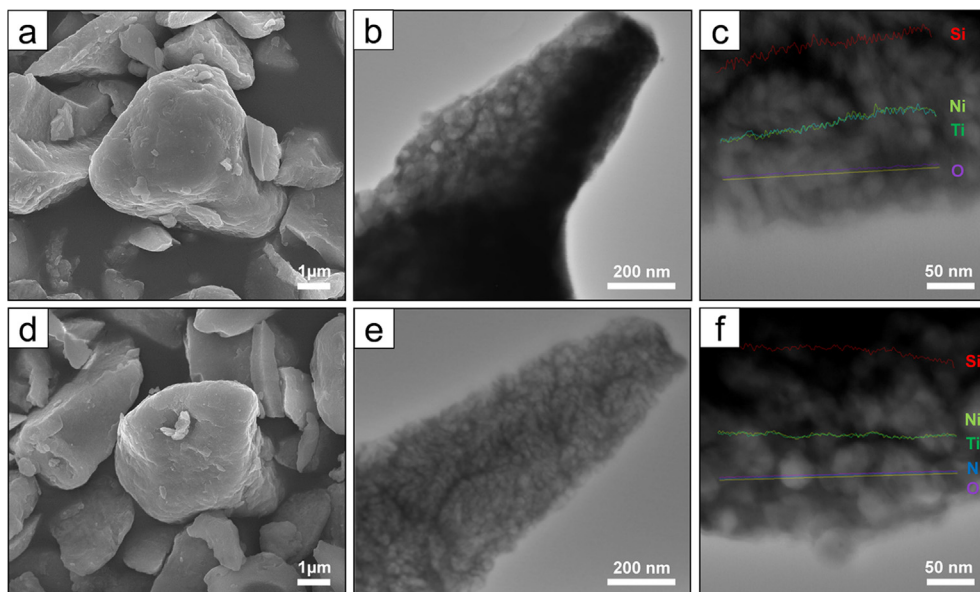


Fig. 1. FE-SEM, TEM, and STEM images of pristine STN particle ((a)–(c)), and nitridated STN particle ((d)–(f)), respectively.

Fig. 2 shows the voltage profiles at the first cycle, cycle retentions and rate capabilities for pristine STN and nitrated STN electrodes. The electrochemical performances were evaluated in the voltage range of 0.01 and 2.0 V (vs. Li/Li^+). As shown in Fig. 2(a) and (b), both electrodes exhibit a long voltage plateaus around 0.1 V, corresponding to the alloying reaction of the crystalline Si with lithium. The pristine STN electrode exhibits the first charge capacity (lithium insertion) of 814 mAh g^{-1} and discharge capacity (lithium removal) of 746 mAh g^{-1} , which indicates the first coulombic efficiency of 91.6%. The nitrated STN electrode

exhibits 12% increased first charge capacity (916 mAh g^{-1}) and 14% increased reversible capacity (849 mAh g^{-1}) compared to those of pristine STN electrode with the first coulombic efficiency of 92.7%. Previously reported STN electrodes showed low initial coulombic efficiencies of around 87%. The increased charge capacity of the nitrated STN electrode is mainly attributed to the enhanced electronic conductivity of STN particles. Although the STN particle is composed of highly conducting metals such as Ti and Ni, its surface is covered by insulating native oxides. Therefore, even if a conducting agent is employed for the conducting path in the electrode, some regions in the electrode are electrically isolated due to the imperfect dispersion of the active material and the conducting agent, which leads to a decrease in capacity. Another possible reason for the increased specific capacity could be the formation of $\text{NiN}_x/\text{NiN}_x\text{O}_y$ compound, which has higher specific capacity and better lithium reversibility than NiO_x . However, the increment in the specific capacity from the $\text{NiN}_x/\text{NiN}_x\text{O}_y$ compound would not be significant due to its marginal existence on the surface of the STN particle. The nitride compounds on the surface of nitrated STN particles also benefit the formation of a stable solid electrolyte interphase layer on the STN particle, which leads to the improvement in coulombic efficiency. The cycle performances for both electrodes were also monitored at a rate of 1 C for 100 cycles. Pre-cycling at a rate of 0.01 C for 3 cycles was performed prior to evaluating the long term cyclability. The pristine and nitrated STN electrodes show the capacity retentions of 70.2% and 74.7%, respectively. It should be noted that even though the nitrated STN electrode shows higher specific capacity, implying that the nitrated STN electrode experiences more severe volume change during cycling compared to the pristine STN electrode, the nitrated STN electrode also exhibits better cycle performance. The excellent mechanical properties of $\text{SiN}_x/\text{SiO}_x\text{N}_y$, such as a high elastic modulus and hardness, suppress the pulverization of the Si active material and improve the mechanics associated with lithium. The rate capability of the pristine STN and nitrated STN electrodes was evaluated at various C rates to explore the effect of nitridation treatment on kinetics (Fig. 3(c)). The nitrated STN electrode shows excellent rate performance compared to that of pristine STN electrode. Especially at as high rate as 3 C, nitrated STN electrode delivered about 4 folds higher capacity than that of pristine STN electrode. The improved rate capability of nitrated STN electrode is attributed to the formation of highly conducting $\text{TiN}_x/\text{TiO}_x\text{N}_y$ compound. The rate capability of electrode is generally governed by the electronic conductivity and the ionic conductivity in the electrode. As shown in Fig. 1, STN powder has a wide range of particle size distribution from $1 \mu\text{m}$ to $10 \mu\text{m}$. A large particle size could induce a long diffusion distance, which lead to a limited improvement in rate capability. Further improvement in the rate capability can be achieved by reducing the STN particle size.

Galvanostatic intermittent titration technique (GITT) was performed to better understand the effect of the nitridation treatment. Fig. 3(a) and (b) shows the transient voltage profiles for the pristine STN and the nitrated STN electrodes during the first cycle, respectively. A closed-circuit voltage (CCV) and a quasi-open-circuit voltage (QOCV) were obtained after applying a constant current density of 0.25 mA g^{-1} for 15 min and switching off the applied current for 30 min, respectively. The internal resistance was calculated from QOCV and CCV values in each transient step as a function of Li stoichiometry in STN-based electrodes (Fig. 3(c)). The nitrated STN electrode shows lower internal resistance compared to that of the pristine STN electrode during cycling, which implies that the nitridation process on STN anode material enables significant improvement in kinetics associated with charges transfer.

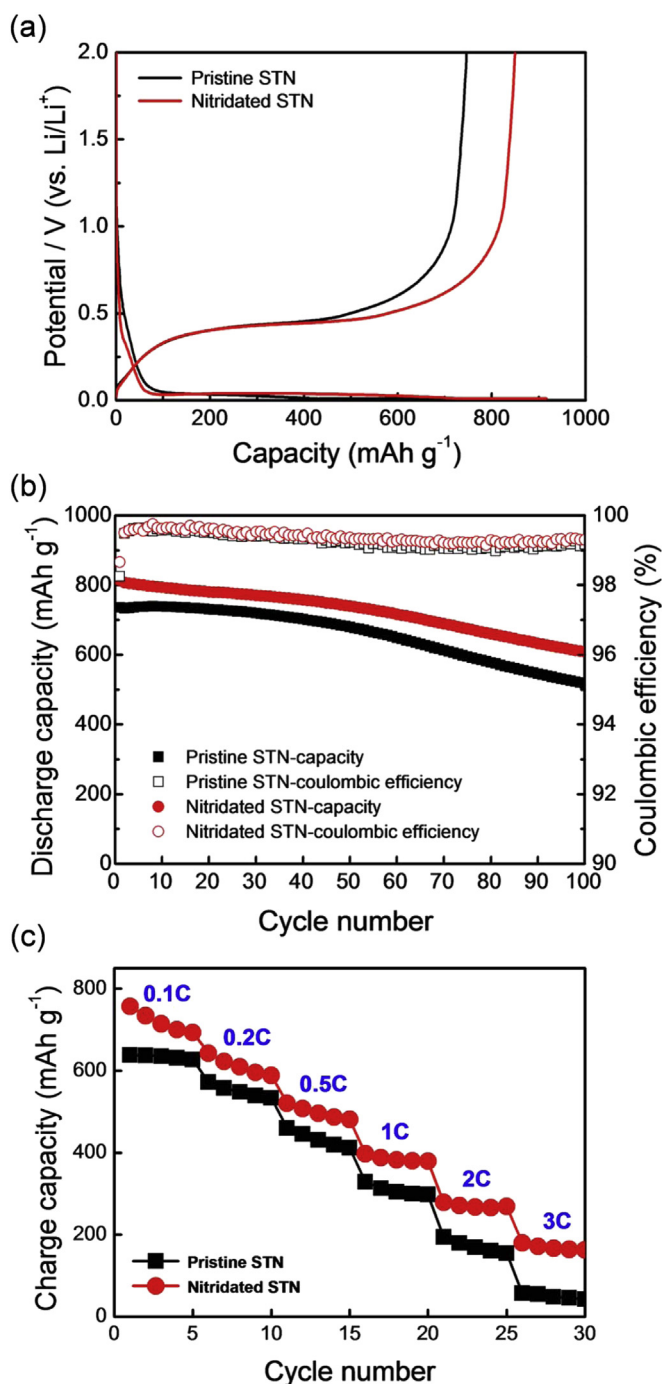


Fig. 2. Electrochemical performances of the pristine STN and the nitrated STN electrodes (a) The first cycle voltage profiles at a rate of 0.1 C. (b) Cycle retentions and coulombic efficiencies at a rate of 1 C. (c) Rate capabilities at various C rates.

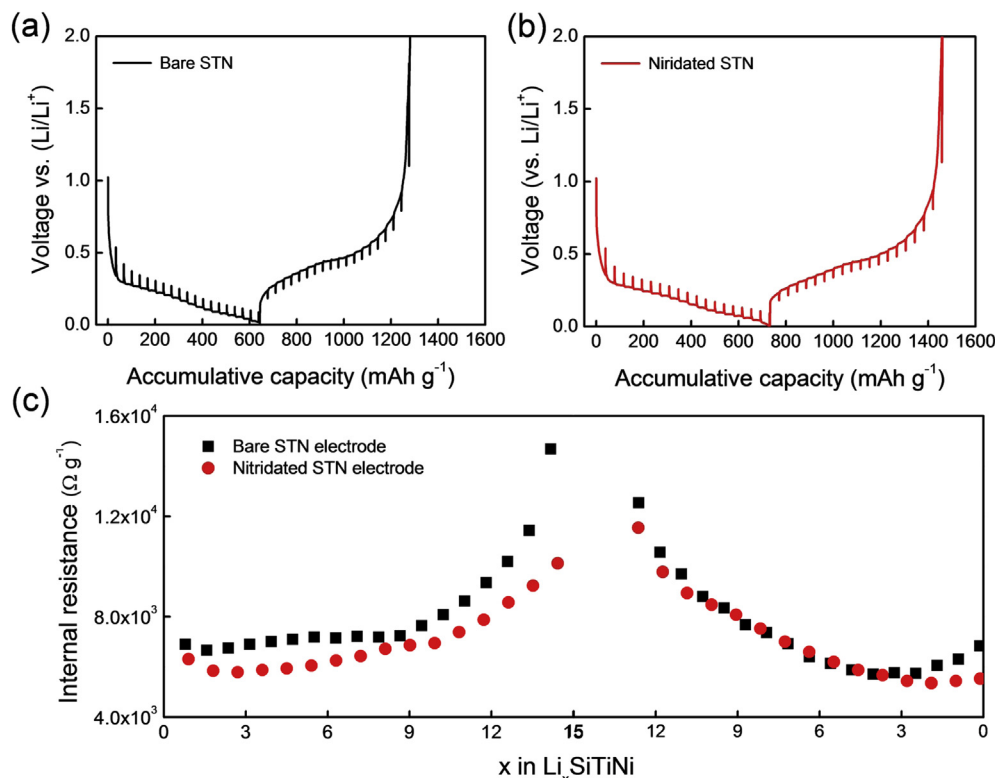


Fig. 3. GITT curves for (a) pristine STN electrode and (b) nitridated STN electrode. (c) Internal resistance data calculated from the transient voltage profile.

4. Conclusion

In conclusion, we have successfully synthesized Si–Ti–Ni alloy sheathed with its nitride compounds, such as SiN_x/SiN_xO_y, TiN_x/TiN_xO_y and NiN_x/NiN_xO_y, using a simple nitridation treatment. The nitride compounds provide a high electric conductivity along the surface as well as mechanical strength, which lead to significant improvements in reversible capacity, cycle performance and rate capability over the pristine STN electrode.

Acknowledgment

This work was supported by the Global Research Laboratory (GRL) Program (K20704000003TA050000310) through the National Research Foundation of Korea (NRF) funded by the Ministry of Science, ICT (Information and Communication Technologies) & Future Planning, and the International Cooperation Program of the Korea Institute of Energy Technology Evaluation and Planning (KETEP) grant funded by the Korea Government of Ministry of Trade, Industry & Energy (2011T100100369).

Appendix A. Supplementary data

Supplementary data related to this article can be found at <http://dx.doi.org/10.1016/j.jpowsour.2013.12.041>.

References

- [1] J.M. Tarascon, M. Armand, *Nature* 414 (2001) 359–367.
- [2] P.G. Bruce, B. Scrosati, J.M. Tarascon, *Angew. Chem. Int. Ed.* 47 (2008) 2930–2946.
- [3] B.A. Boukamp, G.C. Lesh, R.A. Huggins, *J. Electrochem. Soc.* 128 (1981) 725–729.
- [4] H. Kim, M. Seo, M.H. Park, J. Cho, *Angew. Chem. Int. Ed.* 49 (2010) 2146–2149.
- [5] C.K. Chan, H.L. Peng, G. Liu, K. Mcllwraith, X.F. Zhang, R.A. Huggins, Y. Cui, *Nat. Nanotechnol.* 3 (2008) 31–35.
- [6] L.B. Hu, H. Wu, S.S. Hong, L.F. Cui, J.R. McDonough, S. Bohy, Y. Cui, *Chem. Commun.* 47 (2011) 367–369.
- [7] R. Liu, J. Duay, S.B. Lee, *Chem. Commun.* 47 (2011) 1384–1404.
- [8] Y.P. He, C. Brown, Y.Z. He, J.G. Fan, C.A. Lundgren, Y.P. Zhao, *Chem. Commun.* 48 (2012) 7741–7743.
- [9] T. Song, J.L. Xia, J.H. Lee, D.H. Lee, M.S. Kwon, J.M. Choi, J. Wu, S.K. Doo, H. Chang, W. Il Park, D.S. Zang, H. Kim, Y.G. Huang, K.C. Hwang, J.A. Rogers, U. Paik, *Nano Lett.* 10 (2010) 1710–1716.
- [10] Y. Zhao, X.Z. Liu, H.Q. Li, T.Y. Zhai, H.S. Zhou, *Chem. Commun.* 48 (2012) 5079–5081.
- [11] H. Jung, Y.U. Kim, M.S. Sung, Y. Hwa, G. Jeong, G.B. Kim, H.J. Sohn, *J. Mater. Chem.* 21 (2011) 11213–11216.
- [12] S.B. Son, S.C. Kim, C.S. Kang, T.A. Yersak, Y.C. Kim, C.G. Lee, S.H. Moon, J.S. Cho, J.T. Moon, K.H. Oh, S.H. Lee, *Adv. Energy Mater.* 2 (2012) 1226–1231.
- [13] H. Han, T. Song, J.-Y. Bae, L.F. Nazar, H. Kim, U. Paik, *Energy Environ. Sci.* 4 (2011) 4532–4536.
- [14] F. Gillot, J. Oro-Sole, M.R. Palacin, *J. Mater. Chem.* 21 (2011) 9997–10002.
- [15] S.F. Chen, S.J. Zhang, W. Zhao, W. Liu, *J. Nanopart. Res.* 11 (2009) 931–938.
- [16] Z.W. Deng, R. Souda, *Diamond Relat. Mater.* 11 (2002) 1676–1682.
- [17] H.G. Hu, A.H. Carim, *J. Electrochem. Soc.* 140 (1993) 3203–3209.